Deprotonation of the Horse Liver Alcohol Dehydrogenase−NAD^+ Complex Controls Formation of the Ternary Complexes†

Elena G. Kovaleva‡ and Bryce V. Plapp*

Department of Biochemistry, The University of Iowa, Iowa City, Iowa 52242

Received May 11, 2005; Revised Manuscript Received July 23, 2005

ABSTRACT: Binding of NAD^+ to wild-type horse liver alcohol dehydrogenase is strongly pH-dependent and is limited by a unimolecular step, which may be related to a conformational change of the enzyme−NAD^+ complex. Deprotonation during binding of NAD^+ and inhibitors that trap the enzyme−NAD^+ complex was examined by transient kinetics with pH indicators, and formation of complexes was monitored by absorbance and protein fluorescence. Reactions with pyrazole and trifluoroethanol had biphasic proton release, whereas reaction with caprate showed proton release followed by proton uptake. Proton release (200−550 s^{-1}) is a common step that precedes binding of all inhibitors. At all pH values studied, the rate constants for proton release or uptake matched those for formation of ternary complexes, and the most significant quenching of protein fluorescence (or perturbation of adenine absorbance at 280 nm) was observed for enzyme species involved in deprotonation steps. Kinetic simulations of the combined transient data for the multiple signals indicate that all inhibitors bind faster and tighter to the unprotonated enzyme−NAD^+ complex, which has a p*K* of about 7.3. The results suggest that rate-limiting deprotonation of the enzyme−NAD^+ complex is coupled to the conformational change and controls the formation of ternary complexes.

The various reactions in the mechanism of horse liver alcohol dehydrogenase (ADH)[1] are strongly pH-dependent (*1*, *2*). For example, the bimolecular association of NAD^+ is most rapid at low pH below a p*K* of about 9.2 for free (apo)enzyme (*3*, *4*), whereas the unimolecular dissociation of the enzyme−NAD^+ complex is most rapid below a p*K* of 7.6 for the complex (*4*). Binding of NAD^+ is a two-step reaction, where the bimolecular association is followed by a limiting unimolecular step that may be related to the change in conformation between apoenzyme and holoenzyme (ternary complexes) that has been characterized by X-ray crystallography (*3*, *5*−*7*). The limiting rate constant for NAD^+ association decreases as pH is lowered below a p*K* value of 7.6 (*3*).

A variety of studies attributed the p*K* values of 9.2 and 7.6 to ionization of the zinc-water in the active site (*1*, *8*−*10*), but microscopic assignment is uncertain because the zinc-water is linked by a hydrogen-bonded system to His-51 on the surface of the protein (*11*). This hydrogen-bonded system, with a water between Ser-48 and His-51, is also present in the apoenzyme (unpublished, see RCSB entry 1YE3.pdb). Substitution of His-51 with Gln only modestly affects enzymatic activity but decreases the rate constants and alters the pH dependence for binding of NAD^+ (*12*). In the doubly substituted H51Q/K228R enzyme, the catalytic zinc-water appears to be the only ionizable group of the enzyme that could contribute to the pH dependence, and the bimolecular rate constant for binding of NAD^+ and the limiting unimolecular isomerization are faster at high pH where the zinc-water would be unprotonated and make a favorable electrostatic interaction in the "closed" conformation of the enzyme (*1*, *7*, *13*). Deprotonation of the zinc-water may be rate-limiting for binding of NAD^+ and may be required for formation of the ternary complexes.

Previous studies showed that binding of NAD^+ or NAD^+ and 2,2,2-trifluoroethanol (TFE) is accompanied by proton release with rate constants of 250−280 s^{-1} and that quenching of protein fluorescence during binding of NAD^+ occurs with a rate constant of 300−500 s^{-1} (*8*, *14*). It was suggested that the proton release and the conformational change of the enzyme were coincident. However, these studies used a limited set of concentrations that would not isolate the rate-limiting steps. Further studies on the pH dependence of inhibition led to the suggestion that the deprotonated enzyme−NAD^+ complex binds TFE most effectively. In contrast, studies on the pH dependence of the rate of dissociation of TFE from the enzyme−NAD^+−TFE complex let to the suggestion that TFE must bind most rapidly to the protonated enzyme−NAD^+ complex (*15*).

Thus, several questions remain to be answered about proton transfers in the mechanism of ADH. How fast are the protons released during binding of NAD^+ and formation of ternary complexes? Does proton release control the conformational change or vice versa? Do various ligands (alcohols or inhibitors) bind faster to the protonated or to

† This work was supported by NIH Grant AA00279.

* Corresponding author. Address: Department of Biochemistry, 4-712 Bowen Science Building, The University of Iowa, Iowa City, IA 52242-1109. Tel, 319-335-7909; fax, 319-335-9570; e-mail, bv-plapp@uiowa.edu.

‡ Current address: Department of Biochemistry, University of Minnesota, 321 Church St., Minneapolis, MN 55455.

[1] Abbreviations: ADH, liver alcohol dehydrogenase; H51Q, His-51 to Gln substitution; K228R, Lys-228 to Arg substitution; TFE, 2,2,2-trifluoroethanol; Fl, protein fluorescence.

10.1021/bi050865v CCC: $30.25
Published on Web 09/01/2005

the unprotonated enzyme−NAD^+ complex? How much does His-51 contribute to the magnitudes of the reaction rates? These questions were addressed by studying the transient kinetics of proton release and uptake for reactions of wild-type ADH with NAD^+ and inhibitors with different ionization properties, which provide key information for mechanistic interpretation of the data. Transient progress curves were obtained with varied concentrations of ligands, using multiple signals (proton release with indicator dyes, protein fluorescence, coenzyme absorbance, and ternary complex absorbance). Global simulation and fitting of multiple traces were used to evaluate chemically appropriate mechanisms that include proton transfer steps. The results define the kinetic mechanism for binding of NAD^+, proton transfer steps, and formation of the ternary complexes.

EXPERIMENTAL PROCEDURES

Materials. Li-NAD^+ (grade I) was obtained from Roche Molecular Biochemicals. Pyrazole (98%) and 2,2,2-trifluoroethanol (99%) were purchased from Aldrich. Capric acid sodium salt (98%) was from Fluka Chemika. Phenol red and thymol blue sodium salts (ACS reagent grade) were purchased from ICN Biomedicals, Inc. Other reagents were Certified A.C.S.

Protein Purification. The wild-type enzyme was expressed in *Escherichia coli* XL1-Blue strain containing the plasmid pBPP/*Eq*ADH (*16*). The enzyme was purified by a published procedure (*16*), except that 10 mM Tris-HCl and 0.25 mM EDTA, pH 7.9 (at 4 °C), buffer was used for developing the DEAE-Sepharose column. The concentration of enzyme active sites (N, normality) was determined by titration with NAD^+ in the presence of 10 mM pyrazole (*17*).

Transient Kinetics. Transient kinetics were studied with the BioLogic SFM 3 stopped-flow spectrophotometer (dead-time 2.4 ms), and concentrations of ligands were varied systematically. Coenzyme binding in the presence of pyrazole was followed by the increase in absorbance at 293 nm due to formation of the enzyme−NAD^+−pyrazole complex (*17*). Binding was also followed by quenching of protein fluorescence (λ_{ex} = 293 nm, λ_{em} = 310−384 nm). Transient fluorescence data were corrected for the inner filter effect due to NAD^+ by using a standard curve that relates tryptophan fluorescence output in the presence of varied concentrations of NAD^+. Coenzyme binding in the presence of caprate was also followed by an increase in absorbance at 280 nm observed in the difference spectrum of the enzyme−NAD^+−caprate complex (*18*). Due to absorbance of the enzyme at 280 nm (A = 0.455 mL mg^{-1} cm^{-1}), concentrations of NAD^+ only up to about 0.22 mM could be used to keep the total absorbance less than 1.2. Proton release or uptake was followed by the decrease or increase in absorbance of phenol red (559 nm) and thymol blue (596 nm). The extinction coefficients for deprotonated species of phenol red and thymol blue were determined to be ϵ_{559} = 56.1 ± 0.4 mM^{-1} cm^{-1} and ϵ_{596} = 29.2 ± 0.3 mM^{-1} cm^{-1}, respectively, whereas the protonated species did not absorb significantly at these wavelengths.

The reactions were carried out in solutions of low-buffering capacity, containing 10−20 μM pH indicator, 0.25 mM EDTA, and 10−30 μN enzyme as the only buffering species and 33 mM Na_2SO_4 to maintain an ionic strength of 0.1 M. Concentrated enzyme (about 10 mg/mL) was dialyzed extensively under N_2 atmosphere against carbonate-free low-capacity buffer at pH 8 (4 °C). Separate, degassed buffer solutions containing NAD^+, trapping agent or dialyzed enzyme, and indicator were titrated to the desired pH at 25 °C with NaOH under N_2 atmosphere immediately prior to stopped-flow experiments.

Stoichiometry of Protons Released. Enzyme solutions used for stopped-flow experiments were titrated to determine the number of protons released per active site of ADH during formation of the enzyme−NAD^+−inhibitor complex. The solution of the enzyme and the indicator in the buffer used for stopped-flow experiments was sealed in a cuvette under N_2, and the change in absorbance of the pH indicator upon addition of standardized HCl was followed spectrophotometrically. The resulting standard curves were used to determine the amount of acid necessary to change the absorbance of the indicator from the initial to the final value observed in stopped-flow progress curves. The change in absorbance of indicator as a function of acid added to the solution was nearly linear over the range of absorbance changes found in the transient progress curves, and thus, an apparent extinction coefficient could be used to convert the absorbance change to proton production. The following equation was used to estimate the final pH of the transient reaction: $pH_f = pK_{ind} - [\log((I_o(10^{(pK_{ind}-pHo)} + 1) - I_f)/I_f)]$, where pK_{ind} is the pK value for the pH indicator, and I_o and I_f are initial and final concentrations of deprotonated indicator. At each experimental pH value, amplitudes of at least 30 progress curves at varied concentrations of NAD^+ were used to calculate the concentration of protons released.

The release of protons upon binding of NAD^+ to the enzyme was also followed by measuring changes in pH after addition of NAD^+ to the enzyme solution in the presence of pyrazole. Solutions of enzyme (80−100 μN) with 6.7 mM pyrazole were titrated under an N_2 atmosphere with NAD^+, and changes in pH after each addition of NAD^+ were measured. The concentration of protons released was determined by raising the pH to the initial value with 0.1 N NaOH and back-titrating the solution with standardized 0.01 or 0.1 N HCl to the final pH value. At each experimental pH, the concentrations of protons released was normalized to the concentration of the active sites of ADH.

Data Analysis. Stopped-flow progress curves were fitted to a function for a single or a double exponential followed by a linear term using the BioKine software. The apparent kinetic constants, k_{app} and k_{app}/K_S, were determined from the fit of the observed rate constants at varied concentrations of either NAD^+ or inhibitor to the expression $k_{obs} = k_{app}[S]/(K_S + [S])$ using the HYPER program (*19*). The observed rate constants for the reaction of the enzyme with varied concentrations of both NAD^+ and inhibitor (I) were fitted to the equation for a sequential bi mechanism $k_{obs} = k_{lim} \cdot [NAD^+][I]/(K_{ia}K_I + K_{NAD}[I] + K_I[NAD^+] + [NAD^+][I])$ using the SEQUEN program (*19*). A nonlinear least-squares analysis program NONLIN (*20*) was used to fit pH dependencies of the kinetic constants and proton stoichiometry data. The apparent kinetic constants (k_{app}) were fitted to the equation $k_{app} = k_{max}/(1 + K/[H^+])$, which describes a mechanism with one ionizable group where only the protonated form is active (Scheme 1). The proton stoichiometry data were fitted to the equation $[H^+]/[E]_{obs} = ([H^+]/[E]_{max})/$

Scheme 1

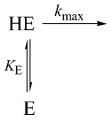

$(1 + K_E/[H^+])$, which describes a mechanism with one ionizable group in the free enzyme and maximal proton release at low pH (Scheme 2).

Scheme 2

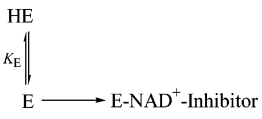

Mechanism Simulations. Kinetic simulation and fitting program Dynafit (*21*) was used to fit transient progress curves for reactions of the enzyme with NAD^+ and inhibitors (pyrazole, TFE, and caprate). To improve the signal-to-noise ratio, progress curves were averaged prior to fitting. For reaction with each trapping agent, averaged traces at varied concentrations of NAD^+ and inhibitor were simulated and fitted to different mechanisms for formation of the enzyme−NAD^+−inhibitor complexes to obtain a single set of microscopic rate constants that describe the data. Although no buffer was added to the reaction solutions (so that transient changes in proton concentration could be measured), the enzyme, pH indicator, and EDTA have some buffering capacity. To account for this buffering, auxiliary equilibria for a macroscopic buffer component and for ionization of water (Scheme 3) were included in the fitting of transient

Scheme 3

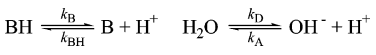

data to all mechanisms.

For reactions at pH 8, the ratio of the protonated (BH) and unprotonated (B) buffering species was calculated from the Henderson−Hasselbalch equation: $pH = pK_B + \log([B]/[BH])$, where pK_B is the apparent p*K* value for phenol red (7.94). During fitting, the microscopic rate constants for protonation (k_{BH}) and deprotonation (k_B) were fixed to values of 10^{10} M^{-1} s^{-1} and 115 s^{-1}, respectively. The effective concentrations of the buffering species were calculated to agree with the average observed change in the indicator absorbance during the transient reaction. The concentrations of protonated (BH) and unprotonated (B) buffer species were 0.0573 and 0.0683 mM for reaction with caprate and 0.0346 and 0.0412 mM for reactions with TFE and pyrazole. For reactions with each inhibitor, transient progress curves for measuring proton release/uptake were fitted using an output factor (apparent extinction coefficient) for unprotonated buffer species (4.32 mM^{-1} cm^{-1}, caprate; 6.51 mM^{-1} cm^{-1}, TFE; 7.52 mM^{-1} cm^{-1}, pyrazole) for the change in absorbance at 559 nm due to changes in concentration of the unprotonated form of phenol red indicator (B). The reaction for ionization of water (Scheme 3) was also included as part of the fitting mechanism to relate concentrations of protons and hydroxide, both of which appear as parts of the mechanisms for reaction of ADH with NAD^+ and trapping agents. The microscopic rate constants for proton association (k_A) and proton dissociation (k_D) were fixed at values of 1.4×10^{11} M^{-1} s^{-1} and 2.5×10^{-5} s^{-1} (*22*). At pH 8, the initial concentrations of H^+, OH^-, and H_2O were fixed at 10^{-8}, 10^{-6}, and 55.5 M, respectively.

Transient progress curves for quenching of protein fluorescence were fitted using output factors for all enzyme species that appear in a particular mechanism, whereas during fitting of the data for the increase in absorbance at 280 nm, an output factor for NAD^+ was included in addition to enzyme species. Reactions giving an increase in absorbance at 293 nm due to the enzyme−NAD^+−pyrazole complex were fitted with an output factor for the final ternary complex (6.60 mM^{-1} cm^{-1}).

A stepwise approach was used in the analysis of the transient data for reaction with each trapping agent. Progress curves for each spectrophotometric signal (i.e., fluorescence, A_{293}, A_{280}, or A_{559}) were fitted separately to various mechanisms for formation of the enzyme−NAD^+−inhibitor complex. The microscopic rate constants for reaction of ADH with NAD^+ and an inhibitor were allowed to vary, as were the output factors that quantify each signal. The microscopic rate constants for auxiliary equilibria (buffer and water) were fixed to the values stated above. After a satisfactory fit of the data for each signal was obtained for a mechanism, the data sets for different signals were combined for a simultaneous fitting. Simultaneous fitting of progress curves from different spectrophotometric signals to the same mechanism was carried out as described, except that the output factors for appropriate species were fixed to the values determined from the individual fits.

RESULTS

Dependence of Proton Release on Concentration of NAD^+ and on pH. Proton release during binding of NAD^+ to wild-type ADH was studied in the presence of saturating concentrations (10 mM) of pyrazole, which traps the enzyme−NAD^+ complex as the ternary enzyme−NAD^+−pyrazole complex. Binding of pyrazole to the enzyme−NAD^+ complex results in an increase in absorbance at 293 nm (*17*) due to formation of a partial covalent bond between N1 of pyrazole and C4 of the nicotinamide ring of NAD^+ (*23*, *24*). In this complex, the water bound to zinc is displaced by the pyrazole and the pyrazole must be deprotonated.

At each pH and concentration of NAD^+, the transient progress curves for the changes in absorbance due to the complex or the indicator fit first-order kinetics (data not shown, but similar traces are shown later). The apparent rate constants exhibited hyperbolic dependence on the concentration of NAD^+ and were fit with HYPER to obtain the maximum rate constant (k_{app}) and the associated bimolecular rate constant (k_{app}/K_{NAD}). A decrease in indicator absorbance due to release of protons in solution was observed only when NAD^+ was present in addition to pyrazole. The rate constants for proton release are comparable in magnitude to the rate constants for the formation of the enzyme−NAD^+−pyrazole complex across the range of pH values (Figure 1). The correspondence indicates that proton release and formation of the ternary enzyme−NAD^+−pyrazole complex are kinetically coupled and may be controlled at the same step in the reaction.

The overall rate constants for the bimolecular reaction of NAD^+ (k_{app}/K_{NAD}) in the formation of the enzyme−NAD^+−

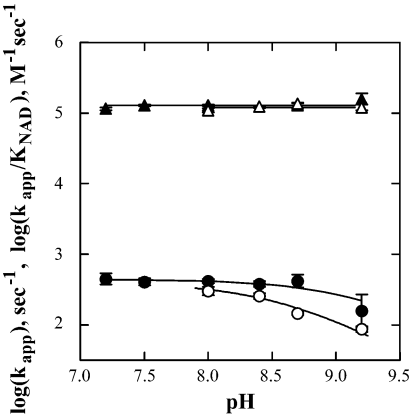

FIGURE 1: pH dependence of the kinetic constants for transient proton release and for formation of the ADH−NAD^+−pyrazole complex. The apparent kinetic constants for proton release (k_{app}, ●; k_{app}/K_{NAD}, ▲) and for formation of the enzyme−NAD^+−pyrazole complex (k_{app}, ○; k_{app}/K_{NAD}, △) in the reaction with NAD^+ and 10 mM pyrazole. The pK values for k_{app} were fitted to the equation $k_{app} = k_{max}/(1 + K/[H^+])$ for the mechanism in Scheme 1. For proton release, the pK value was 9.2 ± 0.3 with k_{max} of 440 ± 30 s^{-1}. For formation of ternary complex (A_{293}), the pK value was 8.6 ± 0.4 with k_{max} of 400 ± 300 s^{-1}. (These parameters are not well-determined, but the data show that the rate constants are similar for proton release and formation of ternary complex.) The k_{app}/K_{NAD} data were pH-independent, with average values of 120 ± 10 mM^{-1} s^{-1} (A_{293}) and 130 ± 10 mM^{-1} s^{-1} (proton release). Reactions were carried out in 33 mM Na_2SO_4, 0.25 mM EDTA, and about 10 μM pH indicator (phenol red or thymol blue) at 25 °C under N_2 atmosphere.

pyrazole complex given in Figure 1 are about 10-fold slower than the previous results that were obtained using phosphate or phosphate/pyrophosphate buffers (*3*, *4*). The present work used 33 mM sodium sulfate to maintain ionic strength and diminish electrostatic effects and to permit proton release studies. Most anions inhibit the binding of NADH to ADH (*25*, *26*), and sulfate appears to inhibit binding of NAD^+. In contrast, the limiting constant (k_{app}) is not significantly different in phosphate/pyrophosphate or sulfate solutions, which would be consistent with a unimolecular isomerization of the enzyme−NAD^+ complex.

Coupling of Proton Transfer to Formation of the Ternary Complexes. The rate-limiting isomerization during NAD^+ binding (studied in the presence of pyrazole) may be controlled by deprotonation or a conformational change, even though there is no direct evidence that the change in conformation between the open and closed forms of the enzyme complexes (as observed by X-ray crystallography) is coupled simply to the binding of NAD^+ (*6*). Formation of ternary complexes may also depend on proton transfers and the conformational state of the enzyme. The mechanism was examined further by studying the binding of varied concentrations of NAD^+ and different inhibitors (pyrazole, TFE, and caprate, all competitive with substrate alcohols) at pH 8. The reactions were monitored by multiple spectrophotometric signals that could report on different forms of enzyme.

Selected transient results for formation of the enzyme−NAD^+−caprate complex are presented in Figure 2. Proton transfer (Figure 2A,B) was biphasic, with an initial rapid release of protons followed by proton uptake. The observed rate constants for the two phases of proton transfer differ in their magnitudes and in their dependence on concentration

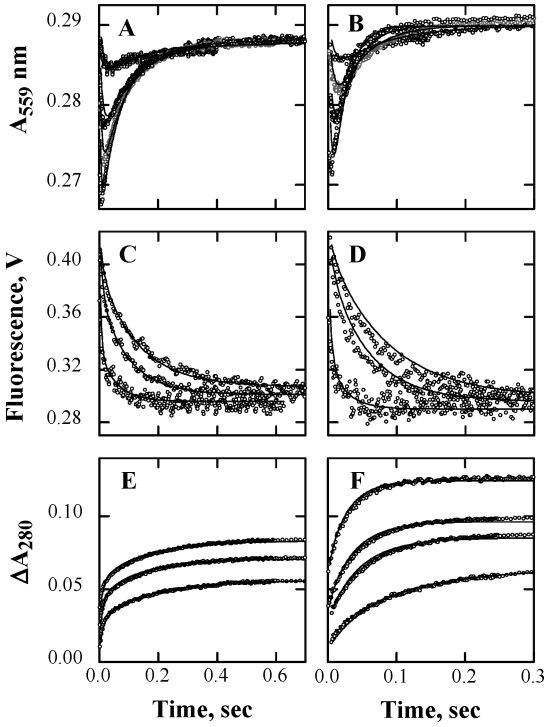

FIGURE 2: Transient and simulated progress curves for reaction of ADH with NAD^+ and caprate. Points are experimental, and lines are simulated progress curves for absorbance at 559 nm due to proton release/uptake (A and B), protein fluorescence (C and D), and absorbance at 280 nm (E and F). For the various signals, enzyme (A_{559}, 7.9 μN; Fl, 2.6 μN; A_{280}, 24.5 μN) was allowed to react with (A) 0.048, 0.17, 0.42, and 1.8 mM NAD^+ and 0.04 mM caprate; (B) 0.074, 0.17, 0.43, and 3.1 mM NAD^+ and 0.15 mM caprate; (C) 0.080, 0.14, and 0.75 mM NAD^+ and 0.05 mM caprate; (D) 0.072, 0.12, and 1.7 mM NAD^+ and 0.12 mM caprate; (E) 0.072, 0.096, and 0.12 mM NAD^+ and 0.04 mM caprate; (F) 0.05, 0.10, 0.12, and 0.17 mM NAD^+ and 0.50 mM caprate (traces top to bottom for (A−D), and bottom to top for (E, F). For clarity, data are not shown for an additional 18 reactions over the concentration ranges of 0.05−2.4 mM NAD^+ and 0.049−0.50 mM caprate, although the data were used in the global fitting. The lines are calculated using estimated microscopic rate constants from Table 3, fitted to the mechanism in Scheme 4. The reaction was carried out in 33 mM Na_2SO_4, 0.25 mM EDTA, and 10 μM phenol red, pH 8.0, at 25 °C under N_2 atmosphere.

of caprate. As illustrated in Figure 3A, the proton release phase (I) shows hyperbolic dependence on the concentration of NAD^+ and appears to be independent of the concentration of caprate, whereas the proton uptake phase (II) was saturable with respect to concentrations of both NAD^+ and caprate (Figure 3B). The data for proton release during formation of the ternary complex with caprate were fitted to the appropriate kinetic equations, and the kinetic constants are given in Table 1. The biphasic proton release/uptake results provide critical information, which indicates that there are two proton transfer steps, and facilitates a mechanistic interpretation of the proton release kinetics with the other inhibitors.

The transient data for quenching of protein fluorescence (Figure 2C,D) and increase in absorbance at 280 nm (apparently due to perturbation of the absorption of the adenine ring of NAD^+, Figure 2E,F) with caprate were biphasic at lower concentrations, indicating that multiple processes and enzyme species also contribute to these spectral signals. The observed rate constants for protein fluorescence and absorbance at 280 nm were in good agreement with those

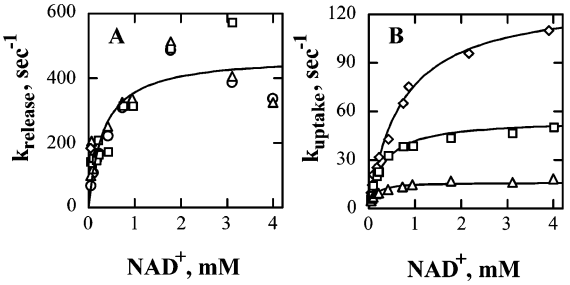

FIGURE 3: Dependence of the observed rate constants for proton release and uptake during reaction of ADH with NAD^+ and caprate. The reaction of enzyme (7.9 μN), NAD^+, and 0.01 (○), 0.04 (△), 0.15 (□), and 0.50 (◇) mM caprate was followed by a change in absorbance of phenol red (10 μM) at 559 nm. The observed rate constants were determined from the fit of transient progress curves (such as in Figure 2) to a double exponential function. (A) The observed rate constants for proton release (phase I) were fitted to the equation for the hyperbolic dependence on concentrations of NAD^+: $k_{obs} = k_{lim}[NAD^+]/(K_{NAD} + [NAD^+])$. (B) The observed rate constants for proton uptake (phase II) were fitted to the equation for the sequential bi mechanism: $k_{obs} = k_{lim}[NAD^+][Cap]/(K_{ia}K_{Cap} + K_{NAD}[Cap] + K_{Cap}[NAD^+] + [NAD^+][Cap])$.

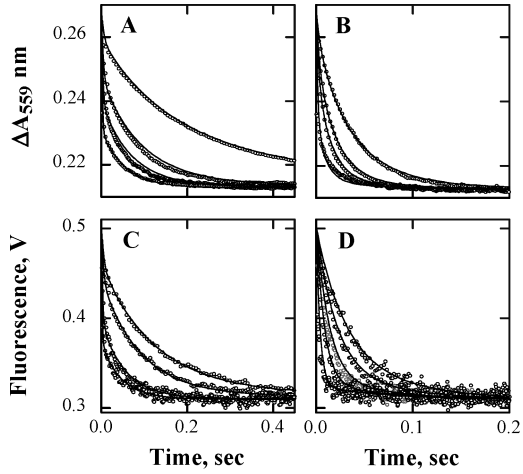

FIGURE 4: Transient and simulated progress curves for reaction of ADH with NAD^+ and TFE. Points are experimental, and lines are simulated progress curves for absorbance at 559 nm due to proton release (A and B) and protein fluorescence (C and D). The enzyme (A_{559}, 8.9 μN; Fl, 2.5 μN) was allowed to react with (A) 0.046, 0.16, 0.35, and 1.5 mM NAD^+ and 0.21 mM TFE; (B) 0.095, 0.21, 0.36, and 2.5 mM NAD^+ and 1.0 mM TFE; (C) 0.069, 0.12, 0.44, and 1.5 mM NAD^+ and 0.21 mM TFE; (D) 0.045, 0.067, 0.11, 0.20, and 0.70 mM NAD^+ and 5.14 mM TFE (traces top to bottom). For clarity, data for an additional 22 reactions over the concentration ranges 0.05−2.6 mM NAD^+ and 0.05−5.1 mM TFE are not shown, but the data were used in fitting. The lines were calculated using the microscopic rate constants from Table 3, fitted to the mechanism in Scheme 5.

for proton transfer at the corresponding concentrations of NAD^+ and caprate. However, rate constants and amplitudes could not be accurately determined for the first phase at higher concentrations of NAD^+, and thus, only the limiting kinetic constants representing phase II of the reaction could be determined (Table 1).

Representative transient reaction data for binding of NAD^+ and TFE are presented in Figure 4. Proton release (Figure 4A,B) is perceptively biphasic, and two rate constants could be extracted from each progress curve. The kinetic constants calculated from the concentration dependences are presented in Table 1. As for the results with caprate, phase I was independent of the concentration of inhibitor, whereas phase II followed sequential kinetics. The magnitudes of the limiting kinetic constants from phase I for NAD^+ binding (k_{lim} and k_{lim}/K_{NAD}) were similar to those for binding of NAD^+ in the presence of caprate, suggesting that the same reaction is involved. Quenching of protein fluorescence was also biphasic, but rate constants for only one phase could be calculated. These depended on concentrations of both ligands and had magnitudes similar to the second phase of proton release.

Representative data for the reaction of ADH with NAD^+ and pyrazole are given in Figure 5, where proton release, protein fluorescence, and the formation of the final enzyme−NAD^+−pyrazole complex (ΔA_{293}) were monitored. Proton release was biphasic at low concentrations of pyrazole, but accurate rate constants were only calculated for phase II, and these were described by a sequential bi mechanism (Table 1). Quenching of protein fluorescence was also biphasic, where the rate constants for phase I depended on

Table 1: Kinetic Constants for Reaction of Alcohol Dehydrogenase with NAD^+ and Inhibitors[a]

signal	phase	k_{lim} (s^{-1})	k_{lim}/K_{NAD} ($mM^{-1}\,s^{-1}$)	k_{lim}/K_I ($mM^{-1}\,s^{-1}$)	K_{NAD} (mM)	K_{ia} (mM)	K_I (mM)
			Caprate				
A_{559}	I[b]	470 ± 30	1500 ± 200		0.32 ± 0.07		
	II[c]	340 ± 40	190 ± 10	410 ± 20	1.8 ± 0.2	0.03 ± 0.03	0.8 ± 0.1
Fl	II[c]	310 ± 30	325 ± 30	1400 ± 100	0.9 ± 0.2	0.3 ± 0.1	0.22 ± 0.04
A_{280}	II[b,d]		215 ± 6	640 ± 170			
			Trifluoroethanol				
A_{559}	I[b]	400 ± 70	900 ± 160		0.5 ± 0.2		
	II[c]	1050 ± 160	640 ± 70	320 ± 40	1.6 ± 0.4	0.3 ± 0.2	3.3 ± 0.9
Fl	II[c]	1100 ± 270	640 ± 50	220 ± 20	1.8 ± 0.5	0.16 ± 0.06	5 ± 1.5
			Pyrazole				
A_{559}	II[c]	130 ± 7	430 ± 60	200 ± 20	0.29 ± 0.05	0.2 ± 0.1	0.6 ± 0.1
Fl	I[b]	210 ± 30	1100 ± 200		0.20 ± 0.07		
	II[c]	120 ± 20	450 ± 100	90 ± 36	0.3 ± 0.1	0.1 ± 0.1	1.3 ± 0.8
A_{293}	II[c]	190 ± 10	350 ± 30	130 ± 10	0.53 ± 0.08	0.18 ± 0.07	1.5 ± 0.2

[a] The apparent first-order rate constants from the single or double exponential fit of the transient data for reaction of the wild-type enzyme with varied concentrations of NAD^+ and inhibitors were fitted to the equations for concentration dependence. [b] For hyperbolic dependence on concentration of NAD^+, $k_{obs} = k_{lim}[NAD^+]/(K_{NAD} + [NAD^+])$. [c] For the sequential bi mechanism, $k_{obs} = k_{lim}[NAD^+][I]/(K_{ia}K_I + K_{NAD}[I] + K_I[NAD^+] + [NAD^+][I])$, where I is the inhibitor. [d] A limiting rate could not be determined because high concentrations of NAD^+ could not be used at that wavelength. Reactions were carried out in 33 mM Na_2SO_4, 0.25 mM EDTA, and 10 μM phenol red at pH 8.0 and 25 °C under N_2 atmosphere.

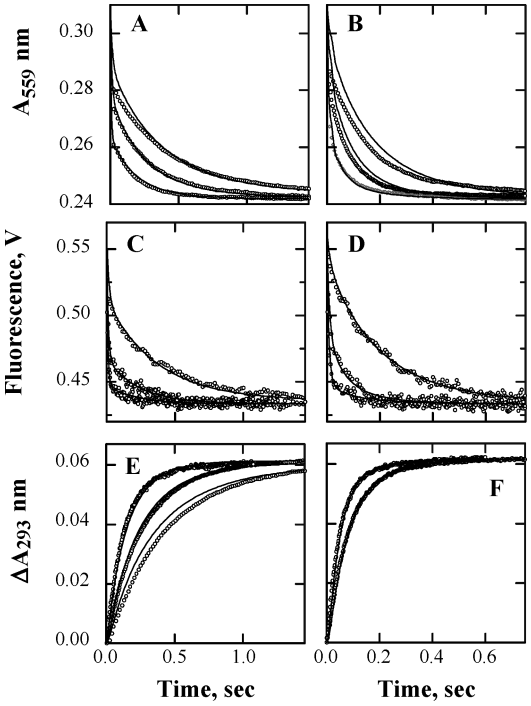

FIGURE 5: Transient and simulated progress curves for reaction of ADH with NAD^+ and pyrazole. Points are experimental, and lines are simulated progress curves for absorbance at 559 nm due to proton release (A and B), protein fluorescence (C and D), and absorbance at 293 nm (E and F). The enzyme (A_{559}, 9.5 μN; Fl, 2.7 μN; A_{293}, 9.5 μN) was allowed to react with (A) 0.088, 0.20, and 0.81 mM NAD^+ and 0.071 mM pyrazole; (B) 0.064, 0.15, and 0.71 mM NAD^+ and 0.25 mM pyrazole; (C) 0.066, 0.20, and 0.36 mM NAD^+ and 0.071 mM pyrazole; (D) 0.043, 0.19, and 0.45 mM NAD^+ and 0.25 mM pyrazole; (E) 0.088, 0.20, and 2.5 mM NAD^+ and 0.071 mM pyrazole; (F) 0.18 and 0.62 mM NAD^+ and 0.25 mM pyrazole (traces top to bottom (A−D), and bottom to top (E and F)). For clarity, data for an additional 20 reactions with concentrations over the ranges 0.09−2.5 mM NAD^+ and 0.07−3.0 mM pyrazole are not shown, but the data were used for fitting. The lines were calculated using the microscopic rate constants from Table 3, fitted to the mechanism in Scheme 5.

the concentration of NAD^+, but not on the concentration of pyrazole, and phase II depended on concentrations of both ligands. The signal at 293 nm showed only a single phase, and the rate constants were described by the sequential bi mechanism.

The results from the studies with the three inhibitors and the multiple signals show two common patterns. The initial transient phase (I) depends on the concentration of NAD^+, but not on the concentration of inhibitor, and has similar kinetic constants for the unimolecular step, k_{lim}, of 210−470 s^{-1} and for the bimolecular reaction, k_{lim}/K_{NAD}, of 900−1500 mM^{-1} s^{-1} for the three inhibitors. The fast phases of proton release with caprate and TFE correspond with the fast phase for quenching of protein fluorescence with pyrazole. These results are consistent with a two-step mechanism for binding of NAD^+, where a bimolecular association is followed by a unimolecular step (e.g., deprotonation or isomerization). The second phase (II) depends on the concentrations of both ligands, and the kinetic constants are specific for each inhibitor. Thus, the magnitudes of k_{lim}, k_{lim}/K_{NAD}, and k_{lim}/K_I for caprate binding are similar when monitored by either proton release, protein fluorescence, or absorbance at 280 nm. Likewise, these kinetic constants are similar for TFE binding as monitored by proton

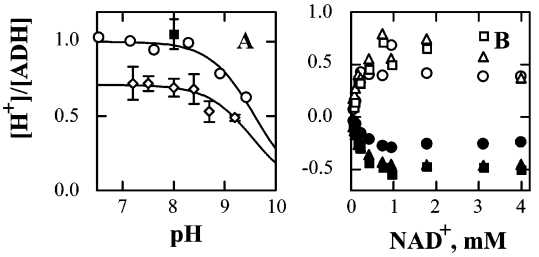

FIGURE 6: Stoichiometry of proton release and uptake during formation of the ADH−NAD^+−inhibitor complexes. (A) At each pH, the number of protons released was determined from the amplitudes of transient progress curves for reaction of the enzyme (8.7−11.7 μN) with NAD^+ (0.05−1.2 mM) and pyrazole (10 mM) in the presence of different pH indicators (◇) and by potentiometric titration of the enzyme (103 μN) with NAD^+ (0−0.5 mM) in the presence of pyrazole (6.7 mM) (○). Lines are fits of the data to the equation $[H^+]/[E]_{obs} = ([H^+]/[E]_{max})/(1 + K_E/[H^+])$ for the mechanism in Scheme 2 using the nonlinear least-squares fitting program NONLIN (*20*). For proton stoichiometry data from transient reactions, the pK_E value was 9.5 ± 0.1 with $[H^+]/[E]_{max}$ of 0.71 ± 0.04, whereas for data from potentiometric titration, the pK_E value was 9.6 ± 0.1 with $[H^+]/[E]_{max}$ of 0.96 ± 0.03. Proton stoichiometry during transient reaction of the enzyme (8.9 μN) with NAD^+ (0.05−3.1 mM) and TFE (0.21−5.1 mM) in the presence of 10 μM phenol red (■) was 1.05 ± 0.1. (B) The stoichiometry of proton release and uptake during transient reaction of the enzyme (7.9 μN) with NAD^+ and 0.01 (○/●), 0.04 (△/▲), and 0.15 (□/■) mM caprate in the presence of 10 μM phenol red at pH 8.0. Reactions were carried out in 33 mM Na_2SO_4 and 0.25 mM EDTA, at 25 °C under N_2 atmosphere.

release or fluorescence and for pyrazole binding as detected by three different signals. That the second phase has kinetic constants that differ for the three inhibitors indicates that this phase is associated with formation of the ternary complexes, which may involve proton transfers and isomerization of ternary complexes. Uptake of protons in the reaction with the anionic inhibitor (caprate) as compared to release of protons in the reactions with inhibitors that deprotonate upon binding (pyrazole and TFE) clearly indicates that the second kinetic phase (II) depends on the inhibitor. The differences in the inhibitors will be analyzed with simulations below.

Stoichiometry of Proton Transfer. The number of protons transferred per active site of enzyme during formation of the enzyme−NAD^+−inhibitor complexes in the transient kinetic reactions and by direct titrations was determined. The pH dependence of the concentration of protons released per active site of the enzyme, $[H^+]/[E]$, can provide apparent pK values for the free enzyme and the final enzyme−NAD^+−inhibitor complex, based on the change in protonation during formation of the complex. For reaction of ADH with NAD^+ in the presence of a saturating concentration of pyrazole, an apparent pK value of 9.6 for the free form of the enzyme and a maximum of about 1 proton released were determined by direct titration, and similar results were obtained from analysis of transient amplitudes from the stopped-flow experiments (Figure 6A). Release of a single proton suggests that deprotonation of a specific group rather than a cumulative release of protons accompanies formation of the ternary complex, and the results agree with previously reported potentiometric data for the reaction of ADH with NAD^+ and either pyrazole or trifluoroethanol (*8*, *27*). The pH profile for proton stoichiometry shown in Figure 6A is consistent with the chemistry of binding of pyrazole, which

results in formation of coordinate bonds between N1 of pyrazole and the catalytic zinc and between N2 of pyrazole and C4 of the nicotinamide ring of NAD^+ (*23*, *24*). The pyrazole proton has a greatly decreased p*K* in the complex (*28*), and only the deprotonated form of pyrazole in the ternary complex should be observed in the pH range of 6.5−10.

In contrast to the reactions with pyrazole and TFE, where deprotonation of both the enzyme−NAD^+ complex and the inhibitor in the ternary complex contribute to the observed release of protons, the anionic inhibitor caprate does not change its protonation state upon forming the ternary complex and, therefore, does not contribute to the proton stoichiometry of the reaction. As shown in Figure 6B, the stoichiometry of proton release and uptake for reaction with caprate exhibits saturable dependence on concentrations of NAD^+, and the nearly equal and opposite amplitudes are consistent with deprotonation and reprotonation of the same group. The net change during transient reaction was about 0.2 protons released, whereas a net change of near 0 was reported previously for potentiometric titration of the enzyme with NAD^+ and caprate (*8*).

The different methods used to determine proton stoichiometry may account for the small differences in the maximum number of protons transferred. Potentiometric titration measures the total pH change for reaction, whereas stopped-flow experiments detect only observable transients, and some amplitude may be lost in accounting for the dead-time for the faster reactions. Nevertheless, the stoichiometry provides information for the mechanistic interpretation of the transient data.

Simulations of the Kinetic Mechanisms. The results show that proton release is kinetically coupled to the rate-limiting step in the formation of the enzyme−NAD^+−inhibitor complex and that there are two kinetically relevant proton transfers associated with binding of NAD^+ and inhibitor. Although the data in Table 1 describe the results mathematically, they do not define the mechanism. The rate constants obtained from the fits to the single or double exponential equations are relaxation constants that are generally complex functions of several microscopic rate constants. A mechanism must be established to account for the rate constants and amplitudes that are observed. To determine the simplest pH-dependent mechanisms that describe formation of the ternary complexes, transient data for reactions with each inhibitor were analyzed using the kinetic simulation program Dynafit (*21*). In this analysis, the data from the progress curves were fitted to various mechanisms, and rate constants and output factors (e.g., extinction coefficients for enzyme species) were obtained. An example of the stepwise approach used in the analysis is illustrated by the studies with caprate.

The simplest mechanism that can describe the transient reaction of ADH with NAD^+ and caprate is depicted in Scheme 4 (see Table 2), where the major pathway for reaction requires deprotonation of the enzyme−NAD^+ complex prior to binding of caprate and subsequent proton uptake that corresponds to protonation of the hydroxide that is displaced. Progress curves for each data set obtained from one spectrophotometric signal were fitted to this mechanism, and the microscopic rate constants and the output factors for species that contribute to the amplitudes were allowed to vary. As shown in Table 2, the microscopic rate constants

Table 2: Estimated Rate Constants for Transient Reaction of Alcohol Dehydrogenase with NAD^+ and Caprate Monitored by Multiple Spectrophotometric Signals[a]

Scheme 4

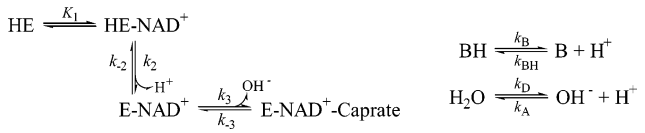

	fluorescence	A_{280}	A_{559}
K_1 (mM)[b]	0.66	0.67	(0.67)
k_2 (s^{-1})	235 ± 9	183.7 ± 0.1	258 ± 2
k_{-2} ($nM^{-1}\,s^{-1}$)	3.4 ± 0.3	4.275 ± 0.005	5.73 ± 0.08
pK_2[c]	7.16 ± 0.04	7.367 ± 0.001	7.347 ± 0.007
k_3 ($mM^{-1}\,s^{-1}$)	330 ± 15	400.7 ± 0.8	432 ± 2
k_{-3} ($\mu M^{-1}\,s^{-1}$)	1.7 ± 0.1	1.70 ± 0.01	1.50 ± 0.03
traces (number)	26	16	12

[a] The stopped-flow data (Figure 2) for reaction of ADH with varied concentrations of NAD^+ and caprate at pH 8.0 were fitted to Scheme 4 above, which combines the mechanism for formation of the ternary complex and auxiliary ionization equilibria, using the program Dynafit (*21*). [b] The equilibrium dissociation constant for NAD^+ (K_1) was calculated from the ratio of the fitted microscopic rate constants for association and dissociation, which were highly correlated, whereas their ratio remained constant. The value of K_1 for data at A_{559} was fixed during fitting. [c] The p*K* values for ionization of the enzyme−NAD^+ complex were calculated from the fitted microscopic rate constants for proton release (k_2) and proton association (k_{-2}) steps, $pK_2 = -\log(k_2/k_{-2})$, and the errors were calculated by propagation of the errors determined for the microscopic rate constants.

determined from the separate fits of the fluorescence, absorbance (A_{280}), or proton release/uptake (A_{559}) data are similar, indicating that the same processes are represented by each signal. Data sets were then combined for simultaneous fitting, and only the rate constants were allowed to vary, whereas the output factors were fixed to the values already determined. The global fits for the data with caprate are given in Table 3. The simulated progress curves calculated from the results of the global fit of the data are represented as the lines in Figure 2, and the good agreement indicates that transient data are explained well by the mechanism in Scheme 4.

The reliability of the fitted microscopic rate constants for reaction with caprate is reinforced by their agreement with previously determined values. For example, the pseudo-first-order rate constant for dissociation of caprate (k_{-3}*[OH^-]) from the ternary complex at pH 8 is 1.7 s^{-1}, similar to the values of 2−4 s^{-1} determined by displacement experiments in the pH range 5.5−8 (*15*). The calculated equilibrium dissociation constant for caprate (k_{-3}*[OH^-]/k_3) at pH 8 of about 4 μM is in good agreement with the values of 7−10 μM determined by spectrophotometric titration (*18*) and inhibition studies (*8*).

A similar approach was used in global fitting of transient data for reaction of ADH with NAD^+ and either pyrazole or TFE. The minimal mechanism required to describe both reactions is depicted in Scheme 5 (see Table 3), where the inhibitor can bind to either the protonated or the unprotonated form of the enzyme−NAD^+ complex. Although Scheme 5 includes the deprotonation step designated by K_5, this step was not included explicitly in the simulation because the dissociation constant can be calculated from the other three steps in the linked equilibria. Furthermore, when the simulation included all four steps, the fitting was unstable as it

Table 3: Summary of Estimated Rate Constants for Transient Reactions of Alcohol Dehydrogenase with NAD^+ and Inhibitors[a]

Scheme 5

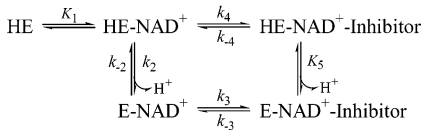

	caprate	pyrazole	TFE
K_1 (mM)[b]	0.62	0.67	0.67
k_2 (s^{-1})	222 ± 4	205 ± 2	551 ± 4
k_{-2} ($nM^{-1}\,s^{-1}$)	4.4 ± 0.2	3.59 ± 0.06	12.4 ± 0.3
pK_2[c]	7.30 ± 0.02	7.24 ± 0.01	7.35 ± 0.01
k_3 ($mM^{-1}\,s^{-1}$)	440 ± 10	136 ± 1	148 ± 2
k_{-3} (s^{-1})	1.73 ± 0.07[d]	0.10 ± 0.01	0.37 ± 0.03
k_4 ($mM^{-1}\,s^{-1}$)	NS[e]	21.1 ± 0.4	11.1 ± 0.4
k_{-4} (s^{-1})	NS[e]	5.7 ± 0.1	15.2 ± 0.8
pK_5[f]		4.68 ± 0.05	4.61 ± 0.05
data traces (number)	39	37	39

[a] The stopped-flow data for reaction of ADH with varied concentrations of NAD^+ and inhibitors were obtained in 33 mM Na_2SO_4, 0.25 mM EDTA, and 10 μM phenol red buffer, pH 8.0, at 25 °C under N_2 atmosphere. The data were analyzed using the program Dynafit (*21*) as described in Experimental Procedures, except that fluorescence data for reaction with pyrazole could not produce a reasonable set of output factors for all enzyme species independently. Therefore, output values for the free enzyme and for the unprotonated form of the enzyme−NAD^+−pyrazole complex were fixed to the values based on the initial and final fluorescence observed for progress curves, and the values for intermediate species were adjusted manually. Scheme 5 (above) shows the overall mechanism for formation of the ternary complexes. For reaction with caprate, transient data for quenching of protein fluorescence, increase in absorbance at 280 nm (A_{280}), and change in absorbance of phenol red (A_{559}) due to release/uptake of protons (e.g., Figure 2) were fitted to the mechanism in Scheme 4. For reaction with pyrazole or TFE, transient data for quenching of protein fluorescence, increase in absorbance at 293 nm (pyrazole), and change in absorbance of phenol red (A_{559}) due to release of protons (Figures 4 and 5) were fitted simultaneously to the mechanism in Scheme 5 with step 5 omitted. [b] The equilibrium dissociation constant for NAD^+ (K_1) was calculated from the ratio of the fitted microscopic rate constants for association and dissociation, which were highly correlated, whereas their ratio remained constant. [c] The pK values for ionization of the enzyme−NAD^+ complex were calculated from the fitted microscopic rate constants for proton release (k_2) and proton association (k_{-2}) steps, $pK_2 = -\log(k_2/k_{-2})$, and the errors were calculated by propagation of the errors determined for the microscopic rate constants. [d] Pseudo-first-order rate constant for dissociation of caprate (k_{-3}*[OH^-]) at pH 8. [e] Not significantly fast. [f] The pK values for ionization of the enzyme−NAD^+−inhibitor complex were calculated using the microscopic reversibility principle, $pK_{E-NAD-I} = -\log [(K_2K_3)/K_4]$, where $K_2 = k_2/k_{-2}$, $K_3 = k_3/k_{-3}$, and $K_4 = k_4/k_{-4}$, and the errors were calculated by propagation of the errors determined for the microscopic rate constants.

gave highly correlated rate constants. If any one of the steps in the box was eliminated, the fitting progressed well.

Transient and simulated progress curves for binding of NAD^+ to ADH in the presence of TFE and pyrazole are shown in Figures 4 and 5, respectively, and the estimated microscopic rate constants are given in Table 3. Although good overall fits were obtained for transient reactions with all inhibitors, deviations for proton release data in the presence of pyrazole appear to be more significant (Figure 5A,B). Perhaps the mechanism for reaction with pyrazole should be more complex, and additional deprotonation steps may be required. Nonetheless, the simultaneous fitting of transient fluorescence, absorbance, and proton release data collected at varied concentrations of NAD^+ and pyrazole indicates that the mechanism in Scheme 5 can describe formation of the ADH−NAD^+−pyrazole complex very well.

As presented in Table 3, there is a good agreement between the microscopic rate constants for deprotonation (k_2) and protonation (k_{-2}) of the enzyme−NAD^+ complex determined for reaction with pyrazole with those for reaction with caprate, indicating that ionization of the enzyme−NAD^+ complex with a pK value of 7.3 is a common step in reaction mechanisms involving both trapping agents. For reaction with TFE, the estimated constants for deprotonation (k_2) and protonation (k_{-2}) of the enzyme−NAD^+ complex are about 2-fold faster than those for reaction with pyrazole or caprate, but the pK value was also about 7.3 (Table 3). It is possible that a specific or a nonspecific effect of TFE as a solute resulted in a 2-fold increase in the magnitudes of the microscopic rate constants without affecting the pK. The pK values for the enzyme−NAD^+−pyrazole and the enzyme−NAD^+−TFE complex were calculated using the principle of thermodynamic, linked equilibria, and the values are similar to those estimated previously (*27*, *28*).

In addition to the microscopic rate constants, the apparent extinction coefficients, or fluorescence yields, for different enzyme complexes were also determined from kinetic simulations (Table 4). It is interesting to note that the extent of quenching of intrinsic protein fluorescence (or an increase in A_{280}) is most significant for species involved in deprotonation step(s) in the mechanism. For example, output values for unprotonated binary and ternary complexes (ϵ_{E-NAD^+} and ϵ_{E-NAD^+-I}) are about 30% lower than the values for the corresponding protonated species (ϵ_{HE-NAD^+} and ϵ_{HE-NAD^+-I}). These results, in addition to the similarity of the microscopic (Tables 2 and 3) and kinetic constants (Table 1) for quenching of protein fluorescence and proton transfer, suggest that there is a connection between the state of protonation and the intrinsic protein fluorescence, which most likely reflects changes in conformation.

The simplest mechanisms required to fit the data well are presented in Tables 2 and 3. Several alternative mechanisms for formation of the ternary complexes were considered, but they did not result in a good representation of the transient data. The simplest, two-step mechanism with bimolecular binding of NAD^+ and then an inhibitor is inadequate because it lacks a limiting unimolecular step. Addition of one unimolecular deprotonation step of either the binary or ternary complex is not sufficient to account for biphasic release of protons in the reactions with subsaturating concentrations of pyrazole and TFE. Rather, the mechanism shown in Scheme 5 (Table 3) without including one of the four steps (2, 3, 4, or 5) was required. For reaction with caprate, displacement of hydroxide with the anionic caprate (Scheme 4, step 3) was required to account for the uptake of protons. Mechanisms that included binding of caprate to the protonated form of the binary enzyme−NAD^+ complex must represent a minor pathway for formation of the ternary complex, since inclusion of this step resulted in fitted values for microscopic rate constants close to zero, whereas constants for the major pathway (i.e., via step 3) were not affected. The results indicate that, although pyrazole or TFE bind to both forms of the enzyme−NAD^+ complex, the major pathway is the same as that determined for reaction with caprate, where inhibitor binds to the unprotonated form of the enzyme−NAD^+ complex (Table 3).

Table 4: Extinction Coefficients and Fluorescence Output Factors for Enzyme Complexes during Transient Formation of the Ternary Complexes with Alcohol Dehydrogenase[a]

inhibitor	signal	ϵ_{HE}	ϵ_{HE-NAD^+}	ϵ_{E-NAD^+}	ϵ_{HE-NAD^+-I}	ϵ_{E-NAD^+-I}	ϵ_{NAD^+}
caprate	A_{280}	20.0	21.0	26.72		25.54	3.22
	Fl	169.2	153	116		114.3	
trifluoroethanol	Fl	200.6	216	126	176	124	
pyrazole	Fl	206	188	141	206	158	

[a] The apparent extinction coefficients (mM^{-1} cm^{-1}, for A_{280}) and fluorescence factors (V mM^{-1} cm^{-1}) for enzyme species were determined from the fits of the transient fluorescence and absorbance (A_{280}) data for reaction with caprate (Figure 2), TFE (Figure 4), and pyrazole (Figure 5) using the kinetic simulation program Dynafit as described in Experimental Procedures. Errors are less than 0.9% of the fitted values. The corresponding microscopic rate constants are shown in Table 3.

An ordered mechanism with NAD^+ binding first best fit the data. Binding of inhibitors to the free enzyme is unlikely as the concentrations of inhibitors used produce competitive inhibition against varied concentrations of alcohols as substrate. At pH 8, deprotonation of the free enzyme would be quantitatively insignificant because essentially all of the enzyme (97%) should be protonated when the apparent p*K* for the zinc−water is about 9.5. Inclusion of additional forms of free enzyme into the mechanisms did not alter the estimates of the microscopic rate constants for steps 1−4 in Scheme 5.

DISCUSSION

Deprotonation Controls Formation of Ternary Comlexes. A major conclusion of this study is that the deprotonation of the enzyme−NAD^+ complex is kinetically coupled to the rate-limiting step in the formation of the ternary complexes. A general mechanism that describes the reaction of the wild-type enzyme with NAD^+ and all three inhibitors is depicted in Scheme 6. This mechanism includes a step for the

Scheme 6

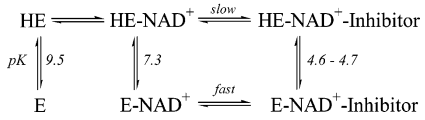

deprotonation of free enzyme, with a p*K* of 9.5, which is derived from the results in Figure 6A, as well as from several studies that show that NAD^+ binds most rapidly to the protonated form of free enzyme (*3*, *4*). The major pathway for formation of the ternary complex involves binding of NAD^+ and the release of a proton, with a p*K* of 7.3, prior to binding of the inhibitor. In the ternary complex, the p*K* is depressed to an unmeasured value of about 4.6 (for pyrazole and TFE), which only indicates that the final species of enzyme is deprotonated at pH 8. The mechanism is similar to ones presented before (*8*, *9*, *29*), but the present results provide rate constants for the steps involved in formation of the ternary complexes so that the major pathway can be described.

It appears that deprotonation of the enzyme−NAD^+ complex (p*K* 7.3) with a rate constant of about 200−550 s^{-1} represents a common, unimolecular step that is rate-limiting in the mechanisms of reaction with all inhibitors. The biphasic proton transfer kinetics with the anionic inhibitor caprate were particularly informative because proton release was followed by proton uptake, and the kinetic steps can be distinguished. In contrast, one proton is lost during formation of the ternary complexes with pyrazole and TFE, and the continuous release of protons was best analyzed with simulations of the full progress curves. The results in Table 3 (Scheme 5) show that inhibitors bind faster (k_3) and tighter (k_{-3}/k_3) to the unprotonated form of the enzyme−NAD^+ complex than to the protonated complex (k_4, k_{-4}/k_4).

These results are consistent with the proposal of Shore and co-workers (*8*) and contrary to the mechanism of Pettersson and co-workers (*1*, *9*, *15*), who concluded that alcohols would bind most rapidly to the protonated enzyme−NAD^+ complex. Kvassman and Pettersson determined the pH dependence of dissociation of TFE and caprate from the ternary complex and used the pH dependence of the binding constant to argue that binding would be most rapid at low pH where the enzyme−NAD^+ complex would be protonated (*15*). However, binding of inhibitor or proton release were not directly measured in those studies.

Kinetic results alone cannot identify the chemical group that deprotonates, but an explanation that is consistent with the chemical mechanism and the structure of ADH involves the catalytic zinc−water and His-51, which are in the hydrogen-bonded network. Although either group in the proton relay system may lose a proton, a reasonable mechanism would have the proton released from the water bound to the catalytic zinc in the enzyme−NAD^+ complex, producing hydroxide that is then displaced in forming the ternary complex. His-51 could facilitate the deprotonation. All three inhibitors coordinate directly to the catalytic zinc and displace the water.

The results for proton stoichiometry support the mechanism for the formation and displacement of zinc-bound hydroxide. At pH 8, perturbation of the p*K* for the catalytic zinc−water from a value of 9.5 to a value of 7.3 upon binding of NAD^+ should result in release of about 0.8 protons per subunit, which is similar to the experimentally determined values of 0.7−1.0 protons released during transient reaction of ADH with NAD^+ and pyrazole or TFE (Figure 6A). For caprate binding, up to 0.7 protons are released in the fast phase, and subsequently, in the slow phase, 0.5 protons are taken up (Figure 6B). This can be explained by protonation of the hydroxide ion that is displaced by caprate from the catalytic zinc (Scheme 4, Table 2).

Although the detailed mechanism for exchange of ligands at the catalytic zinc is not known, the displacement of neutral water from zinc is generally expected to be more rapid than dissociation of negatively charged hydroxide. However, the kinetic results indicate that the inhibitors bind preferentially to the deprotonated form of the enzyme−NAD^+ complex, so that hydroxide rather than water is formally displaced. Two reasonable mechanisms may be proposed.

In one mechanism, the neutral alcohol or pyrazole could bind adjacent to the zinc-bound hydroxide on the same face of the zinc and donate a proton to the hydroxide ion, which would then dissociate as a water molecule. The bound alcohol or pyrazole would be unprotonated, which is consistent with the observed three-dimensional structures (*30*, *24*). In contrast, binding of the anionic caprate to the unprotonated enzyme requires proton uptake, which could occur by protonating the hydroxide with solvent water through the proton relay system so that water dissociates. This mechanism could proceed by formation of a pentacoordinate zinc. Although pentacoordinate zinc has not been observed by X-ray crystallography for complexes of ADH with coenzyme and a substrate or substrate analogue, the complex of apoenzyme with 1,10-phenanthroline is pentacoordinate (*31*).

A second mechanism involves inversion of the zinc coordination and is supported by recent results. The carboxyl group of the conserved Glu-68 is located about 4.7 Å from the catalytic zinc, on the opposite side of the bound water in the apoenzyme structures or the substrate analogue in the ternary complexes. Ryde proposed, on the basis of computational studies, that the carboxyl group could bind to the zinc and displace the water to form a transient four-coordinate complex that would then react with the incoming ligand in a double displacement that restores the original zinc coordination (*32*). Thus, Glu-68 would facilitate the ligand exchange, but it is not known if the hydroxide would be protonated before displacement. Structures of several ADHs have been determined in which the corresponding glutamate residue is ligated to the catalytic zinc in some forms of the enzyme and is in a second sphere position in other complexes. For instance, Glu-60 in the apoenzyme from *Clostridium beijerinckii* is ligated to the zinc (at 2.3 Å), whereas in the complexes with NADP, the distance is 3.8 Å (*33*). Likewise, Glu-69 is ligated to the zinc in the apoenzyme from *Sulfolobus solfataricus* and is in the second sphere when an alcohol binds in the holoenzyme (*34*, *35*). In three of the four subunits in the apoenzyme from *Escherichia coli*, Glu-59 is ligated to the zinc, whereas in the complexes with NAD, the glutamate is displaced and a water on the opposite side ligates to zinc (*36*). In human ADH3 complexed with NAD^+ and decanoate (with the methyl group within van der Waals contact to the zinc), Glu-67 is ligated to the zinc, whereas in the apoenzyme or the abortive NADH-*S*-(hydroxymethyl)-glutathione ternary complex, the glutamate is displaced by water or the substrate (*37*, *38*). In all of these structures, the zinc moves about 2 Å upon the change in coordination, while the other ligands to the zinc (cysteine, histidine, and sometimes aspartic acid residues) undergo small conformational changes.

If the glutamate residue is required for ligand exchange, substitution with another amino acid residue might affect enzymatic activity. In an early mutagenesis study, Glu-67 in the homologous yeast alcohol dehydrogenase was substituted with a glutamine residue, with a corresponding decrease in catalytic efficiency of about 100-fold (*39*). In contrast, substituting Glu-60 with alanine or aspartic acid residues in the enzyme from *Thermoanaerobacter brockii* (very similar to the *C. beijerinckii* enzyme) only decreased catalytic efficiency from 4- to 8-fold (*40*). Interestingly, X-ray absorption fine-structure analysis on the wild-type and mutated enzymes suggests that the zinc is tetracoordinated in the apoenzyme structures, whereas it is pentacoordinated in holoenzyme complexes with $NADP^+$ and the substrate analogue dimethyl sulfoxide. Perhaps a water molecule substitutes for Glu-60 in the mutated enzymes. Additionally, time-resolved X-ray absorption studies of the wild-type enzyme suggest that two different pentacoordinated zinc complexes form during the transient phase of the oxidation of an alcohol (*41*). The conclusion from these studies is that the exchange of a substrate for the zinc-bound water (or hydroxide) is complex and not yet understood.

Conformational Change Is Coincident with Deprotonation. Another conclusion of these studies is that the deprotonation appears to be coupled to the conformational change that is known to occur during formation of ternary complexes. The spectroscopic data do not permit definitive assignments of the conformational states of the enzyme species in the kinetic mechanism. Nevertheless, the changes in protein fluorescence and absorbance at 280 nm lead to the suggestion that step 2 in the mechanisms in Schemes 4 or 5 is associated with structural changes in the protein. The intrinsic protein fluorescence arises primarily from Trp-314, which is buried in the interface between the subunits in the dimeric molecule. Although the environment of Trp-314 is similar in the apo- and holoenzyme conformations, Trp-314 is located near the loop that undergoes rearrangement during the conformational change (*6*, *42*, *43*). The quenching of ADH fluorescence at high pH has been attributed to resonance energy transfer to a group, perhaps Tyr-286, that ionizes with a p*K* of about 9.8 (*44*, *45*), but it is difficult to explain how the p*K* would shift to 7.3 upon binding of NAD^+ since the environment of Tyr-286 does not change during the conformational change observed by X-ray crystallography. The fluorescence quenching events still need spectroscopic explanations (*46*). The pH dependence of fluorescence quenching and the coupling to the binding of NAD^+ and TFE are affected by chemical modifications of residues in the active site, and thus, it was proposed that the common event was a conformational change (*29*). The present results suggest that the change in protein fluorescence is related primarily to the deprotonation of the enzyme−NAD^+ complex (Table 4). The largest changes in fluorescence output factors correspond to the deprotonation of the enzyme species, HE−NAD^+ or HE−NAD^+−I. There are also small effects related to the binding of NAD^+ and binding of the inhibitor. Whether the deprotonation controls the conformational change or vice versa is not resolved with the present data. If the conformational change requires that the zinc−water deprotonate in order for the positively charged nicotinamide ring to bind next to the zinc, the events could be closely coupled.

The increase in absorbance at 280 nm (difference maximum at 281 nm) also seems to report on an event related to the proton transfer (Table 4). The change in A_{280} was initially observed by difference spectroscopy of enzyme−adenosine diphosphate ribose, enzyme−NAD^+−caprate, and enzyme−NADH−isobutyramide complexes (*18*). Perturbation of the adenine spectrum by the hydrophobic and electrostatic environment of the enzyme active site could explain the absorbance change at 280 nm, since this spectral feature could be reproduced in the free coenzyme by changes in pH, salt concentration, and solvent (*47*). In contrast to the static titration experiments, however, the transient kinetics indicate that the origin of this spectral feature is not simply

the binding of the adenine ring, as the deprotonation of HE−NAD^+ to form E−NAD^+ results in the largest increase in A_{280}. Furthermore, transients for reaction of ADH with NAD^+ and caprate were biphasic (Figure 2E), and the correspondence between the observed rate constants for quenching of protein fluorescence, proton uptake, and absorbance at 280 nm suggests that the enhancement of absorbance at 280 nm involves binding of caprate and NAD^+. Even though the structural and spectroscopic origins of the absorbance band at 280 nm are uncertain, it is reasonable to conclude that perturbation of the spectrum reports on changes in protein conformation that accompany formation of binary and ternary enzyme complexes, as does quenching of intrinsic protein fluorescence.

The conformational change during binding of NAD^+ is proposed to be a two-step process that could first involve binding of the AMP or adenosine diphosphoribose portion of the coenzyme followed by positioning of the nicotinamide ring close to the catalytic zinc. X-ray crystallography shows that ternary complexes with NAD^+ and various substrates or inhibitors usually have the "closed" conformation. However, the conformation may remain "open" upon modification (or loss) of the nicotinamide ring of the coenzyme (*48*−*51*), binding of ligands to the catalytic zinc (*48*, *52*), and substitutions of amino acid residues in the active site (*2*, *12*, *53*, *54*), coenzyme-binding domain (*55*), and flexible loop (*43*). In these open structures, the adenosine diphosphoribose portion of the coenzyme is bound in a position similar to that found in closed forms in the various complexes, but the nicotinamide ring (if present) can be in a variety of positions. Many of these modifications also alter the pH profiles for various steps in the catalytic mechanism of ADH, suggesting a connection between the conformational state of the enzyme complex and the protonation state of a group that controls reactivity. Therefore, it is relevant that the most significant changes in the protein fluorescence and absorbance at 280 nm correspond to the deprotonation steps (Table 4). It appears that a global change in protein conformation is coincident with the deprotonation of the enzyme−NAD^+ complex and binding of the nicotinamide ring close to the catalytic zinc−water.

This interpretation is consistent with earlier proposals that the positioning of the nicotinamide ring and the conformation are affected by the state of protonation of the zinc−water (*1*, *7*, *12*, *13*). Thus, deprotonation of the zinc-bound water, facilitated by His-51, may promote formation of the closed conformation of the enzyme−NAD^+ complex by electrostatic attraction of the positively charged nicotinamide ring of NAD^+ to the catalytic zinc−hydroxide. In the holoenzyme conformation, the nicotinamide ring would be less than 4 Å from the zinc−water (if the position of the oxygen in various ligands bound to the zinc is used). However, it may be noted that enzyme depleted of the active site zinc binds NAD^+ similarly to wild-type enzyme (*56*) and crystallizes with NADH in the closed form (*57*). Perhaps ionization of Cys-46 or Cys-174 can compensate for the loss of the zinc−water.

To determine that deprotonation of the zinc−water controls formation of the holo-conformation of the enzyme and that His-51 facilitates proton transfer, His-51 was substituted with Gln, leaving the catalytic zinc−ligand (water or alcohol) as the only ionizable group that might contribute to the reactions in the observable pH range (*2*, *12*). The H51Q enzyme has altered pH dependencies for binding of NAD^+ and alcohol oxidation, but studies on the transient kinetics of proton transfers with H51Q ADH are required to determine the rate constants and if proton transfers are connected to conformational changes.

This work demonstrates directly that proton transfer is important for the mechanism of ADH. Although proton transfer steps are often ignored in enzyme mechanisms, or are considered to be in rapid equilibrium, pH-dependent kinetics suggest that proton transfers should be studied. Proton transfers may be rapid, but may also be rate-limiting in catalysis. The experimental approach used in this study, which uses global simulation of transient progress curves, could be applied to many other enzymes where proton transfers are part of the mechanism.

REFERENCES

1. Pettersson, G. (1987) Liver alcohol dehydrogenase, *CRC Crit. Rev. Biochem. 21*, 349−389.
2. LeBrun, L. A., Park, D.-H., Ramaswamy, S., and Plapp, B. V. (2004) Participation of histidine-51 in catalysis by horse liver alcohol dehydrogenase, *Biochemistry 43*, 3014−3026.
3. Sekhar, V. C., and Plapp, B. V. (1988) Mechanism of binding of horse liver alcohol dehydrogenase and nicotinamide adenine dinucleotide, *Biochemistry 27*, 5082−5088.
4. Kvassman, J., and Pettersson, G. (1979) Effect of pH on coenzyme binding to liver alcohol dehydrogenase, *Eur. J. Biochem. 100*, 115−123.
5. Brändén, C.-I., Jörnvall, H., Eklund, H., and Furugren, B. (1975) Alcohol dehydrogenases, in *The Enzymes* (Boyer, P. D., Ed.), 3rd ed., Chapter 11, pp 103−190, Academic Press, New York.
6. Eklund, H., Samama, J.-P., Wallén, L., Brändén, C.-I., Åkeson, Å., and Jones, T. A. (1981) Structure of a triclinic ternary complex of horse liver alcohol dehydrogenase at 2.9 Å resolution, *J. Mol. Biol. 146*, 561−587.
7. Eklund, H., and Brändén, C.-I. (1987) Alcohol dehydrogenase, in *Biological Macromolecules and Assemblies: Volume 3-Active Sites of Enzymes* (Jurnak, F. A., and McPherson, A., Eds.) pp 73−141, Wiley, New York.
8. Shore, J. D., Gutfreund, H., Brooks, R. L., Santiago, D., and Santiago, P. (1974) Proton equilibria and kinetics in the liver alcohol dehydrogenase reaction mechanism, *Biochemistry 13*, 4185−4191.
9. Kvassman, J., and Pettersson, G. (1980) Unified mechanism for proton-transfer reactions affecting the catalytic activity of liver alcohol dehydrogenase, *Eur. J. Biochem. 103*, 565−575.
10. Evans, S. A., and Shore, J. D. (1980) The role of zinc-bound water in liver alcohol dehydrogenase catalysis, *J. Biol. Chem. 255*, 1509−1514.
11. Eklund, H., Plapp, B. V., Samama, J. P., and Brändén, C.-I. (1982) Binding of substrate in a ternary complex of horse liver alcohol dehydrogenase, *J. Biol. Chem. 257*, 14349−14358.
12. LeBrun, L. A., and Plapp, B. V. (1999) Control of coenzyme binding to horse liver alcohol dehydrogenase, *Biochemistry 38*, 12387−12393.
13. Plapp, B. V., Sogin, D. C., Dworschack, R. T., Bohlken, D. P., Woenckhaus, C., and Jeck, R. (1986) Kinetics of native and modified liver alcohol dehydrogenase with coenzyme analogues: isomerization of enzyme-nicotinamide adenine dinucleotide complex, *Biochemistry 25*, 5396−5402.
14. Shore, J. D., Gutfreund, H., and Yates, D. (1975) Quenching of protein fluorescence by transient intermediates in the liver alcohol dehydrogenase reaction, *J. Biol. Chem. 250*, 5276−5277.
15. Kvassman, J., and Pettersson, G. (1980) Effect of pH on the binding of decanoate and trifluoroethanol to liver alcohol dehydrogenase, *Eur. J. Biochem. 103*, 557−564.
16. Park, D.-H., and Plapp, B. V. (1991) Isoenzymes of horse liver alcohol dehydrogenase active on ethanol and steroids. cDNA cloning, expression, and comparison of active sites, *J. Biol. Chem. 266*, 13296−13302.

17. Theorell, H., and Yonetani, T. (1963) Liver alcohol dehydrogenase−DPN−pyrazole complex: a model of a ternary intermediate in the enzyme reaction, *Biochem. Z. 338*, 537−553.
18. Theorell, H., and Yonetani, T. (1964) Studies on liver alcohol dehydrogenase complexes: IV. Spectrophotometric observations on the enzyme complexes, *Arch. Biochem. Biophys. 106*, 252−258.
19. Cleland, W. W. (1979) Statistical analysis of enzyme kinetic data, *Methods Enzymol. 63*, 103−138.
20. Johnson, M. L., and Frasier, S. G. (1985) Nonlinear least-squares analysis, *Methods Enzymol. 117*, 301−342.
21. Kuzmic, P. (1996) Program DYNAFIT for the analysis of enzyme kinetic data: application to HIV proteinase, *Anal. Biochem. 237*, 260−273.
22. Eigen, M., and De Maeyer, L. (1963) Relaxation methods, in *Techniques of Organic Chemistry* (Friess, S. L., Lewis, E. S., and Weissberger, A., Eds.) pp 895−1054, Wiley (Interscience), New York.
23. Eklund, H., Samama, J.-P., and Wallén, L. (1982) Pyrazole binding in crystalline binary and ternary complexes with liver alcohol dehydrogenase, *Biochemistry 21*, 4858−4866.
24. Rubach, J. K., and Plapp, B. V. (2003) Amino acid residues in the nicotinamide binding site contribute to catalysis by horse liver alcohol dehydrogenase, *Biochemistry 42*, 2907−2915.
25. Olden, B., and Pettersson, G. (1982) Anion binding to liver alcohol dehydrogenase, *Eur. J. Biochem. 125*, 311−315.
26. Adolph, H. W., Kiefer, M., and Cedergren-Zeppezauer, E. (1997) Electrostatic effects in the kinetics of coenzyme binding to isozymes of alcohol dehydrogenase from horse liver, *Biochemistry 36*, 8743−8754.
27. Eftink, M. R., and Bystrom, K. (1986) Studies of the pH dependence of the formation of binary and ternary complexes with liver alcohol dehydrogenase, *Biochemistry 25*, 6624−6630.
28. Andersson, P., Kvassman, J., Lindstrom, A., Olden, B., and Pettersson, G. (1981) Effect of pH on pyrazole binding to liver alcohol dehydrogenase, *Eur. J. Biochem. 114*, 549−554.
29. Parker, D. M., Hardman, M. J., Plapp, B. V., Holbrook, J. J., and Shore, J. D. (1978) pH-Dependent changes of intrinsic fluorescence of chemically modified liver alcohol dehydrogenases, *Biochem. J. 173*, 269−275.
30. Ramaswamy, S., Eklund, H., and Plapp, B. V. (1994) Structures of horse liver alcohol dehydrogenase complexed with NAD^+ and substituted benzyl alcohols, *Biochemistry 33*, 5230−5237.
31. Boiwe, T., and Brändén, C.-I. (1977) X-ray investigation of the binding of 1,10-phenanthroline and imidazole to horse-liver alcohol dehydrogenase, *Eur. J. Biochem. 77*, 173−179.
32. Ryde, U. (1995) On the role of Glu-68 in alcohol dehydrogenase, *Protein Sci. 4*, 1124−1132.
33. Korkhin, Y., Kalb, G., Peretz, M., Bogin, O., Burstein, Y., and Frolow, F. (1998) NADP-dependent bacterial alcohol dehydrogenases: crystal structure, cofactor-binding and cofactor specificity of the ADHs of *Clostridium beijerinckii* and *Thermoanaerobacter brockii*, *J. Mol. Biol. 278*, 967−981.
34. Esposito, L., Sica, F., Raia, C. A., Giordano, A., Rossi, M., Mazzarella, L., and Zagari, A. (2002) Crystal structure of the alcohol dehydrogenase from the hyperthermophilic archaeon *Sulfolobus solfataricus* at 1.85 Å resolution, *J. Mol. Biol. 318*, 463−477.
35. Esposito, L., Bruno, I., Sica, F., Raia, C. A., Giordano, A., Rossi, M., Mazzarella, L., and Zagari, A. (2003) Crystal structure of a ternary complex of the alcohol dehydrogenase from *Sulfolobus solfataricus*, *Biochemistry 42*, 14397−14407.
36. Karlsson, A., el-Ahmad, M., Johansson, K., Shafqat, J., Jörnvall, H., Eklund, H., and Ramaswamy, S. (2003) Tetrameric NAD-dependent alcohol dehydrogenase, *Chem. Biol. Interact. 143−144*, 239−245.
37. Sanghani, P. C., Robinson, H., Bosron, W. F., and Hurley, T. D. (2002) Human glutathione-dependent formaldehyde dehydrogenase. Structures of apo, binary, and inhibitory ternary complexes, *Biochemistry 41*, 10778−10786.
38. Sanghani, P. C., Bosron, W. F., and Hurley, T. D. (2002) Human glutathione-dependent formaldehyde dehydrogenase. Structural changes associated with ternary complex formation, *Biochemistry 41*, 15189−15194.
39. Ganzhorn, A. J., and Plapp, B. V. (1988) Carboxyl groups near the active site zinc contribute to catalysis in yeast alcohol dehydrogenase, *J. Biol. Chem. 263*, 5446−5454.
40. Kleifeld, O., Shi, S. P., Zarivach, R., Eisenstein, M., and Sagi, I. (2003) The conserved Glu-60 residue in *Thermoanaerobacter brockii* alcohol dehydrogenase is not essential for catalysis, *Protein Sci. 12*, 468−479.
41. Kleifeld, O., Frenkel, A., Martin, J. M., and Sagi, I. (2003) Active site electronic structure and dynamics during metalloenzyme catalysis, *Nat. Struct. Biol. 10*, 98−103.
42. Strasser, F., Dey, J., Eftink, M. R., and Plapp, B. V. (1998) Activation of horse liver alcohol dehydrogenase upon substitution of tryptophan 314 at the dimer interface, *Arch. Biochem. Biophys. 358*, 369−376.
43. Ramaswamy, S., Park, D.-H., and Plapp, B. V. (1999) Substitutions in a flexible loop of horse liver alcohol dehydrogenase hinder the conformational change and unmask hydrogen transfer, *Biochemistry 38*, 13951−13959.
44. Wolfe, J. K., Weidig, C. F., Halvorson, H. R., and Shore, J. D. (1977) pH-Dependent conformational states of horse liver alcohol dehydrogenase, *J. Biol. Chem. 252*, 433−436.
45. Eftink, M. R. (1986) Quenching of the intrinsic fluorescence of liver alcohol dehydrogenase by the alkaline transition and by coenzyme binding, *Biochemistry 25*, 6620−6624.
46. Eftink, M. R. (1992) Luminescence studies with horse liver alcohol dehydrogenase: information on the structure, dynamics, transitions and interactions of this enzyme, *Adv. Biophys. Chem. 2*, 81−114.
47. Subramanian, S., Ross, J. B., Ross, P. D., and Brand, L. (1981) Investigation of the nature of enzyme−coenzyme interactions in binary and ternary complexes of liver alcohol dehydrogenase with coenzymes, coenzyme analogues, and substrate analogues by ultraviolet absorption and phosphorescence spectroscopy, *Biochemistry 20*, 4086−4093.
48. Cedergren-Zeppezauer, E., Samama, J. P., and Eklund, H. (1982) Crystal structure determinations of coenzyme analogue and substrate complexes of liver alcohol dehydrogenase: binding of 1,4,5,6-tetrahydronicotinamide adenine dinucleotide and *trans*-4-(*N*,*N*-dimethylamino)cinnamaldehyde to the enzyme, *Biochemistry 21*, 4895−4908.
49. Samama, J. P., Zeppezauer, E., Biellmann, J. F., and Brändén, C.-I. (1977) The crystal structure of complexes between horse liver alcohol dehydrogenase and the coenzyme analogues 3-iodopyridine-adenine dinucleotide and pyridine-adenine dinucleotide, *Eur. J. Biochem. 81*, 403−409.
50. Eklund, H., Samama, J. P., and Jones, T. A. (1984) Crystallographic investigations of nicotinamide adenine dinucleotide binding to horse liver alcohol dehydrogenase, *Biochemistry 23*, 5982−5996.
51. Li, H., Hallows, W. H., Punzi, J. S., Marquez, V. E., Carrell, H. L., Pankiewicz, K. W., Watanabe, K. A., and Goldstein, B. M. (1994) Crystallographic studies of two alcohol dehydrogenase-bound analogues of thiazole-4-carboxamide adenine dinucleotide (TAD), the active anabolite of the antitumor agent tiazofurin, *Biochemistry 33*, 23−32.
52. Cedergren-Zeppezauer, E. (1983) Crystal-structure determination of reduced nicotinamide adenine dinucleotide complex with horse liver alcohol dehydrogenase maintained in its apo conformation by zinc-bound imidazole, *Biochemistry 22*, 5761−5772.
53. Cedergren-Zeppezauer, E. S., Andersson, I., Ottonello, S., and Bignetti, E. (1985) X-ray analysis of structural changes induced by reduced nicotinamide adenine dinucleotide when bound to cysteine-46-carboxymethylated liver alcohol dehydrogenase, *Biochemistry 24*, 4000−4010.
54. Plapp, B. V., Eklund, H., Jones, T. A., and Brändén, C.-I. (1983) Three-dimensional structure of isonicotinimidylated liver alcohol dehydrogenase, *J. Biol. Chem. 258*, 5537−5547.
55. Rubach, J. K., Ramaswamy, S., and Plapp, B. V. (2001) Contributions of valine-292 in the nicotinamide binding site of liver alcohol dehydrogenase and dynamics to catalysis, *Biochemistry 40*, 12686−12694.
56. Dietrich, H., MacGibbon, A. K., Dunn, M. F., and Zeppezauer, M. (1983) Investigation of the pH dependencies of coenzyme binding to liver alcohol dehydrogenase lacking zinc ion at the active sites, *Biochemistry 22*, 3432−3438.
57. Schneider, G., Eklund, H., Cedergren-Zeppezauer, E., and Zeppezauer, M. (1983) Structure of the complex of active site metal-depleted horse liver alcohol dehydrogenase and NADH, *EMBO J. 2*, 685−689.

BI050865V